

1 Non-parabolicity and band gap re-normalisation in Si doped ZnO

2 R. E. Treharne* and L. J. Phillips, K. Durose

3 *Stephenson Institute for Renewable Energy, University of Liverpool, UK*

4 A. Weerakody, I. Z. Mitrovic

5 *Department of Electrical Eng. and Electronics, University of Liverpool, UK*

6 (Dated: October 11, 2013)

Abstract

7 PACS numbers: 78.20.Jq, 88.66.sq, 81.15.-z

8 Keywords: zinc oxide; magnetron sputtering; thin-film; doping; non-parabolicity, band gap normalisation

9 INTRODUCTION

10 EXPERIMENTAL METHODS

11 Films were deposited via RF magnetron sputtering using an AJA Phase II-J Orion system.
12 The system was configured with a 'sputter-up' geometry with the substrate being suspended
13 above two separate ceramic targets of ZnO and SiO₂ that were arranged off-centre and tilted
14 at 5° towards the middle of the substrate. Soda-lime glass substrates (OptiWhiteTM, NSG)
15 of size 100 × 100 × 4 mm³ were used throughout. They were cleaned by scrubbing with a
16 nylon brush and a series of de-ionized water and isopropanol alcohol rinses followed by blow
17 drying with a nitrogen gas jet. During deposition the ZnO and SiO₂ targets were sputtered
18 from simultaneously using powers of 150 W and 50 W respectively. A growth pressure
19 of 2mTorr Ar was used during deposition. The substrate temperature was maintained at
20 350 ± 5°C during growth and the substrate was kept static (i.e was not rotated). Deliberate
21 gradients of both thickness and composition were subsequently achieved across the resultant
22 film to generate a 'combinatorial' sample. A second film of pure SiO₂ was deposited under
23 identical conditions (but without ZnO) to generate a reference film for calculating the % wt.
24 profile of SiO₂ in the co-sputtered film.

25 A Shimadzu UV-Vis-IR 3700 spectrophotometer with mapping capability was used to
26 measure the transmittance of the co-sputtered film over the range 250 - 2500 nm. 289
27 spectra were taken in total at 5 mm increments over the full sample surface. At each of
28 these 289 points the sheet resistance was also measured using a CMT-SR2000 4-point probe
29 mapping system. Following transmittance and sheet resistance measurements the sample
30 was cut into one hundred 10 × 10 mm² pieces. A selection of these pieces, 10 in total,
31 were further scribed into four 5 × 5 mm² sections and Hall measurement were performed on

each of these sections. The Hall measurement was performed with custom built equipment, provided by Semimetrics Ltd., using a field strength of 0.8 T. Ellipsometry was performed on the same sections using a Woollam M2000-UI system. Ellipsometry was also used to map the thickness profile of the pure SiO₂ reference film.

RESULTS

Fitting of optical spectra

Figure 1 shows a typical transmittance spectra taken from a single point on the combinatorial ZnO:Si sample. The full details of the model of the dielectric permittivity, $\varepsilon(\omega)$, used to fit the data are given in [1]. The key components of the model include: 1) a Lorentzian oscillator to account for the behaviour of the system's bound electrons and to provide a smoothly varying dielectric background over the range of interest (250 – 2500 nm), 2) an extended Drude model [2], to characterise the system's free electron response, and 3) an inter-band transition model to account for the steep increase in the material's absorption coefficient ($\alpha \propto (E - E_G)^{1/2}$) in the vicinity of its direct band gap (3.3 – 3.4 eV). The two key parameters extractable from the dielectric model are the film's thickness, d , and plasma frequency, ω_p , which is related directly to the carrier concentration according to

$$\omega_p = \sqrt{\frac{n_e e^2}{m_e \varepsilon_0}} \quad (1)$$

where m_e is the effective electrons (expressed in units of the free electron mass, m_0) and ε_0 is the permittivity of free space.

Fitting was achieved by using a Nelder-Mead downhill simplex algorithm [3], implemented

51 via python script, to minimize the quantity

$$\chi^2 = \sum_i^N \sqrt{\frac{y_i - O_i}{N^2}} \quad (2)$$

52 where N is the total number of data points in the spectra, O_i the observed transmittance at
53 each wavelength over the range of interest, and y_i the theoretical transmittance calculated
54 using the transfer matrix method [4] for a single thin-film on a finite, transparent substrate.
55 The fitting algorithm was iterated until the relative fractional change in consecutive χ^2
56 values was less than 1×10^{-6} . The fitting of all 289 transmittance spectra taken over the
57 combinatorial sample was fully automated, the only user input required being an initial
58 estimate of film thickness at the point of the first spectrum. This automation ensured that
59 the fitting of consecutive spectra was highly consistent. For all spectra, χ^2 values of < 1
60 were achieved indicating that all fits were as successful as that shown in figure 1.

61 It was not possible to extract accurate values for the optical band-gap E_G from the inter-
62 band transition component of the model. All values were typically ~ 0.2 eV lower than
63 expected (even once non-parabolicity and re-normalisation effects had been accounted for,
64 see sections and). This is due to the presence of a population of impurity states located in
65 energy just below the bottom of the conduction band. The presence of these states generate
66 a broadening, commonly referred to as an ‘Urbach tail’ [5], in the onset of the absorption
67 coefficient. It is very difficult to determine the extent of this broadening by fitting the
68 dielectric model to a single transmittance spectra. The use of variable angle spectroscopic
69 ellipsometry (VASE) was therefore necessary to determine the true band gap of the material.

70 For each point over the combinatorial sample surface a set of three ellipsometric spectra,
71 taken at angles of 60, 65 and 70° with respect to a plane normal to the sample surface, was
72 measured and fitted using a parameterized semi-conductor (PSEMI-M0) model [6] over the
73 range 350 – 1000 nm. The use of multiple spectra allowed the effect of the tail states to be

extricated from the direct band to band transitions. Figure 2 shows the difference in the α^2 versus E behaviour extracted from transmittance and ellipsometry data respectively. This disparity between band gaps extracted from the two techniques has been reported previously by Srikant [7].

Conduction band non-parabolicity

For highly doped metal-oxides it has been shown that the conduction band, E_c , is ‘non-parabolic’ and that the origin of this non-parabolicity may be attributed to a carrier dependent effective mass, $m_e(n_e)$. The functional form of this dependence, first suggested by Pisarkiewicz *et. al* [8], is given by

$$m_e(n_e) = m_{e0} \sqrt{1 + \frac{2C\hbar^2 k}{m_{e0}}} \quad (3)$$

where m_{e0} is the value of the effective mass at the conduction band minimum and C is the non-parabolicity factor, expressed in eV^{-1} . The carrier wave-number can be expressed in terms of the carrier concentration according to $k = (3\pi^2 n_e)^{1/3}$. By re-examining equation 1 it is clear that the relationship between ω_p^2 and n_e is becomes non-linear if the effective mass is not a constant. Figure 3 shows a plot of ω_p , extracted from the spectrophotometry measurements, versus the carrier concentration, n_e^H , determined via Hall measurements, for the sample subset cut from the original combinatorial sample. A similar χ^2 minimization procedure to that described in section , in which the fitting parameters were m_{e0} and C , was applied to the data set using

$$\chi^2 = \sum_{i=1}^n \frac{(n_{e_i}^S - n_{e_i}^H)^2}{n^2} \quad (4)$$

where the superscript S corresponds to carrier concentrations calculated, using a carrier dependent effective mass $m_e(n_e)$ (equations (1) a 3), from the spectroscopically determined

94 plasma frequencies. The superscript H denotes values of n_e determined directly via Hall
 95 measurements. To determine the uncertainty associated with the fitted m_{e0} and C values a
 96 Monte-Carlo style error treatment [9] was implemented within which the χ^2 minimization
 97 procedure was performed 1000 times. The inset plot in figure 3 shows the mean $m_e(n_e)$
 98 relationship (solid line) and the corresponding spread (yellow line). An average extracted
 99 value of $m_{e0} = 0.35 \pm 0.02m_0$ is higher than previous published values of $0.24 - 0.28m_0$ for
 100 the effective mass in undoped ZnO. An average extracted value of $C = 0.30 \pm 0.01$ eV agrees
 101 very well with previously reported values of ~ 0.29 eV $^{-1}$ [10, 11] for Al doped ZnO films.

102 **Band-gap renormalization**

103 The optical band gap of a degenerately doped metal-oxide system increases as a function
 104 of carrier concentration (Burstein-Moss shift [12, 13] according to

$$E_G = E_{G0} + \frac{\hbar^2(3\pi^2n_e)^{2/3}}{2m_{eff}} \quad (5)$$

105 where E_{G0} is the band-gap at the conduction band minimum and the joint density of states
 106 effective mass, m_{eff} is given as

$$\frac{1}{m_{eff}} = \frac{1}{m_h} + \frac{1}{m_e(n_e)} \quad (6)$$

107 A constant hole effective mass value of $m_h = 0.7m_0$ [] is assumed throughout this work. Note
 108 that the non-parabolicity of the conduction band is accounted for when estimating the band
 109 gap by using the carrier dependent effective mass $m_e(n_e)$ determined in section . The data
 110 points in figure 4 show the band-gap values, determined via ellipsometry, plotted against the
 111 Hall carrier concentrations. The points lie some distance from the relationship predicted by
 112 equation 5. The apparent reduction in the real band-gap values is due the re-normalization

113 effects of many body electron-electron, electron-ion and hole-hole interactions. Lu *et. al*
 114 [14] have shown that the total energy shift due to re-normalization can be estimated by
 115 parameterising the detailed model described by Jain *et. al* according to

$$E_R = An_e^{1/3} + Bn_e^{1/4} + Cn_e^{1/2} \quad (7)$$

116 where E_R is negative with respect to E_G . The $n_e^{1/3}$, $n_e^{1/4}$ and $n_e^{1/2}$ dependencies correspond to
 117 the exchange energy of free electrons, their correlation energy and the electron-ion interaction
 118 energy respectively. The coefficients A , B , and C , quantify the strength of each of these three
 119 dependencies. The coefficient values for the data shown in figure 4, and a value for E_{G0} , was
 120 extracted using the established minimisation procedure. Table I show the extracted values
 121 and comparative values for n-type ZnO thin-films. The strength of the $n_e^{1/3}$ dependence is
 122 roughly three times than that reported for Al doped ZnO.

123 MAPPING OF COMPOSITIONAL DEPENDENCE

124 Film thickness profiles were determined for the combinatorial ZnO:Si and SiO₂ samples.
 125 The % wt. SiO₂ content at each point over the combinatorial sample was estimated according
 126 to

$$x = \frac{\Gamma_B d_B}{\Gamma_A d_A + \Gamma_B d_B} \times 100\% \quad (8)$$

127 where Γ_A and Γ_B are the bulk densities of ZnO and SiO₂ respectively and d_A and d_B are the
 128 corresponding thicknesses, d , of the ZnO and SiO₂ films. The carrier concentration profile
 129 for the combinatorial sample was calculated from extracted ω_p^S values according to equation
 130 1 and using the non-parabolic effective mass relationship, $m_e(n_e)$, determined in section .
 131 The corresponding mobility profile was calculated according to

$$\mu_e = \frac{1}{n_e^S R_S de} \quad (9)$$

132 where R_S are the sheet resistance values obtained directly from 4 point probe measurements.
 133 Figure 3 shows the three dimensional contour profiles of n_e and μ_e accross the surface of
 134 the combinatorial sample. In both cases, a maximal ridge, corresponding to $n_e \sim 4.5 \text{ cm}^{-3}$
 135 an $\mu_e \sim 16 \text{ cm}^2\text{V}^{-1}\text{s}^{-1}$, runs diagonally across the sample. By superimposing the contour
 136 distribution of % wt. SiO_2 content (dotted black contour lines) a very strong correlation
 137 between carrier concentration and composition becomes apparent, the maximum n_e and μ_e
 138 values corresponding to a value of $x = 0.65\%$ wt. SiO_2 content.

139 By plotting the distributions of n_e and μ_e with respect to x the compositional dependence
 140 can be observed directly, see figure 4. Here the strength of the combinatorial analysis is
 141 fully appreciated by its ability to generate continuous, non-ambiguous distributions of the
 142 material's electrical behaviour and shows that it is highly sensitive to the composition -
 143 the resistivity spanning over three orders of magnitude within the compositional range $x =$
 144 $0 - 0.65\%$ wt. SiO_2 . Furthermore, the uncertainty in the optimum value of x , that minimises
 145 the resistivity, is significantly reduced when compared to the multi-sample analyses that are
 146 commonly reported.

147 The solid straight line in the n_e vs x plot indicates the relationship predicted for a 100%
 148 doping efficiency, i.e. where every Si atom incorporated into film substitutionally replace a
 149 Zn atom and contributes two free electrons to the system. For low values of x , i.e. in the
 150 range $0 - 0.5\%$ wt. SiO_2 , this relationship is adhered to. However as x increases further the
 151 doping efficiency decreases rapidly and the carrier concentration is limited to $3 - 4 \times 10 \text{ cm}^{-3}$
 152 for compositions up to 10% wt. SiO_2 . After the optimum value of x is reached the mobility
 153 drops off steeply and approaches a value of zero for values of x beyond 6%. This suggests
 154 that as x is increased beyond the optimum composition, Si is no longer incorporated into
 155 the film as a substitutional dopant and instead acts to increase the scattering of the free

carriers, existing as an interstitial impurities or forming segregated Si-O phases at the grain boundaries.

Scattering

The behaviour of carrier mobility can be described further by considering its direct relationship with the carrier concentration. Figure 5 shows that by plotting μ_e versus n_e for all data points two distinct populations are revealed. The red data points correspond to compositions $x < 0.65\%$. Within this distribution, and for carrier concentrations below $2.5 \times 10^{16} \text{ cm}^{-3}$ the mobility of the free carriers can be described in terms of a grain barrier limited transport model proposed by Seto *et.al* [15]. The model assumes that at the grain boundaries a population of filled trap states exist within the band gap. This causes the conduction band to bend upwards at each grain boundary forming a barrier to charge transport. The inter-grain mobility, μ_B of free carriers is therefore limited by thermal processes according to

$$\mu_{ig} = \mu_0 \exp\left(-\frac{\Phi_B}{k_B T}\right) \quad (10)$$

where Φ_B is the barrier height at the grain boundary and is related directly to the carrier concentration according to

$$\Phi_B = \frac{e^2 n_t}{8 \varepsilon_\infty \varepsilon_0 n_e} \quad (11)$$

where n_t is the trap density and ε_∞ is the high frequency dielectric permittivity ($\varepsilon_\infty \sim 8.3$ for single crystal ZnO [16]). The pre-factor μ_0 is the internal mobility of the grain, expressed as

$$\mu_0 = \frac{eL}{\sqrt{2\pi m_e k_B T}} \quad (12)$$

174 where L is the grain size. It is necessary to extend the Seto model in the case of degenerately
 175 doped ZnO to account for the tunnelling of carriers through the barrier Φ_B . As the carrier
 176 concentration increases the Fermi level rises towards the top of the barrier while the barrier
 177 height decreases proportionally to $1/n_e$. Following the onset of tunnelling the effective carrier
 178 mobility increases exponentially with respect to carrier concentration. The mobility and is
 179 eventually limited by other scattering processes, for example ionized-impurity scattering. A
 180 semi-empirical relationship the mobility due to the tunnelling of free carriers, μ_t can be
 181 expressed according to

$$\mu_t = \frac{\mu_{ii} - \mu_{ig}}{1 + \exp[-\frac{1}{\alpha}(\Delta_{BM} + E_R - \beta\Phi_B)]} \quad (13)$$

182 where the factor α accounts for the sharpness of the onset in tunnelling and is likely to be
 183 related to the depletion width of the grain boundary. A second empirical factor, β takes into
 184 account of any extra functional dependence of Φ_B on n_t which is likely vary with respect
 185 to n_e . The effective mobility may therefore be expressed as the sum of the inter-grain and
 186 tunnel mobilities according to

$$\mu_{eff} = \mu_{ig} + \mu_t \quad (14)$$

187 Figure 5 shows corresponding the fit of this extended model to the data in the region of
 188 composition $x < 0.65\%$. An extracted value of $n_t = 1.79 \times 10^{14} \text{ cm}^{-3}$ is over two orders of
 189 magnitude greater than that reported for reactively sputtered, undoped ZnO films [17] and
 190 an order of magnitude greater than that for Al doped ZnO films [18]. This is reflected in
 191 the relatively low optimum mobility values of $\sim 16 \text{ cm}^2\text{V}^{-1}\text{s}^{-1}$ which is typically half that
 192 of Al doped ZnO films. The reduction of the level trap densities at the grain boundaries is
 193 therefore key to the improvement of carrier mobility in Si doped ZnO films. This is likely to
 194 be achieved through further investigations of the effect of growth parameters, i.e. substrate

195 temperature and sputter pressure. Based on the model used in this work, a reduction of n_t
196 by *sim20*\$ could yield a doubling of the mobility.

197 The green data points in figure 5 show the n_e versus μ_e behaviour for $> 0.65\%$ wt.
198 SiO₂ compositions. The mobility now tends towards a minimum value at a higher carrier
199 concentration of $\sim 3 \text{ cm}^2\text{V}^{-1}\text{s}^{-1}$. This is indicative of an increased trap density, the result
200 of an excess of Si at the grain boundaries or perhaps the formation of Si-O phases.

201 CONCLUSIONS

202 A consideration of the non-parabolicity of the conduction band for Si doped ZnO has
203 yielded estimates for the values of the band minimum effective mass, $m_{e0} = 0.35m_0$, and the
204 non-parabolicity factor, $C = 0.3 \text{ eV}^{-1}$. The non-parabolicity contributes to a reduction in
205 the expected Burstein-Moss shift of the optical band-gap at carrier concentrations beyond
206 10^{20} cm^{-3} . Further reductions in the band-gap arises from the renormalization effects which
207 are dominated by electron-electron and electron-ion interactions. For Si doped films the
208 component of the magnitude of these effects are significantly greater than that reported for
209 sputtered Al doped ZnO films.

210 The combinatorial methodology employed within this work allows the relationship be-
211 tween composition and the electrical behaviour to be determined with excellent accuracy,
212 with a continuous distributions between n_e , μ_e , ρ and % wt. SiO₂ being determined. Further-
213 more, the extraction of all data from a single sample ensures that a high level of consistency
214 between each data point is achieved compared with measurements taken over a series of
215 separately deposited samples. Maximum values of $4.5 \times 10^{20} \text{ cm}^{-3}$ and $16 \text{ cm}^2\text{V}^{-1}\text{s}^{-1}$ were
216 achieved for the carrier concentration and mobility respectively, at an optimal composition
217 of $x = 0.65\%$ wt. SiO₂, and this corresponding to a minimum resistivity of $8.7 \text{ }\Omega\cdot\text{cm}$.

218 The model of grain boundary scattering proposed by *Seto* [15] has been extended to
 219 include the effects of tunneling through grain boundaries. The model generates a good
 220 agreement for the observed μ_e versus n_e behaviour at compositions up to the optimum value
 221 of x . The model highlights a potential route to improving carrier mobility, i.e. by reducing
 222 the density of trap states that exist at the grain boundaries.

223 Above the optimum composition a different dependence is observed to that below it. This
 224 is thought to be due to the increased density of trap states associated with the incorporation
 225 of excess Si into the films.

226 * Corresponding Author: R.Treharne@liverpool.ac.uk

- 227 [1] R. E. Treharne, K. Hutchings, D. A. Lamb, S. J. C. Irvine, D. Lane, and K. Durose, J. Phys.
 228 D: Appl. Phys **45**, 335102 (2012).
- 229 [2] D. Mergel and Z. Qiao, J. Phys. D: Appl. Phys **35**, 794 (2002).
- 230 [3] J. A. Nelder and R. Mead, The Computer Journal **7**, 308 (1965).
- 231 [4] H. A. Macleod, *Thin-Film Optical Filters* (Adam Hilger Ltd, 1986).
- 232 [5] F. Urbach, Phys. Rev. **92**, 1324 (1953).
- 233 [6] C. Herzinger, B. Johs, W. McGahan, J. Woollam, and W. Paulson, J. Appl. Phys. **83**, 3323
 234 (1998).
- 235 [7] V. Srikant and D. R. Clarke, J. Appl. Phys. **83**, 5447 (1998).
- 236 [8] T. Pisarkiewicz and A. Kolodziej, Phys. Stat. Sol. B **158**, K5 (1990).
- 237 [9] R. J. Mendelsberg, *Photoluminescence of ZnO grown by eclipse pulsed laser deposition*, Ph.D.
 238 thesis, University of Canterbury, New Zealand (2009).
- 239 [10] F. Ruske, A. Pflug, V. Sittering, B. Szyszka, D. Greiner, and B. Rech, Thin Solid Films **518**,

240 1289 (2009), article in press - Thin Solid Films.

241 [11] K. Ellmer, J. Phys. D: Appl. Phys **34**, 3097 (2001).

242 [12] E. Burstein, Phys. Rev. **93**, 632 (1954).

243 [13] T. S. Moss, Proc. Phys. Soc. B **67**, 775 (1954).

244 [14] J. Lu, S. Fujita, T. Kawaharamura, H. Nishinaka, Y. Kamada, T. Ohshima, Z. Ye, Y. Zeng,
245 Y. Zhang, L. Zhu, *et al.*, J. Appl. Phys. **101**, 083705 (2007).

246 [15] J. Y. W. Seto, J. Appl. Phys. **46**, 5247 (1975).

247 [16] N. Ashkenov, B. N. Mbenkum, C. Bundesmann, V. Riede, M. Lorenz, D. Spemann, E. M.
248 Kaidashev, A. Kasic, M. Schubert, and M. Grundmann, J. Appl. Phys. **93**, 126 (2003).

249 [17] P. F. Carcia, R. S. McLean, M. H. Reilly, and G. Nunes, App. Phys. Lett. **82**, 1117 (2003).

250 [18] M. Kon, P. Song, Y. Shigesato, P. Frach, S. Ohno, and K. Suzuki, Jpn. J. App. Phys. **42**,
251 263 (2003).

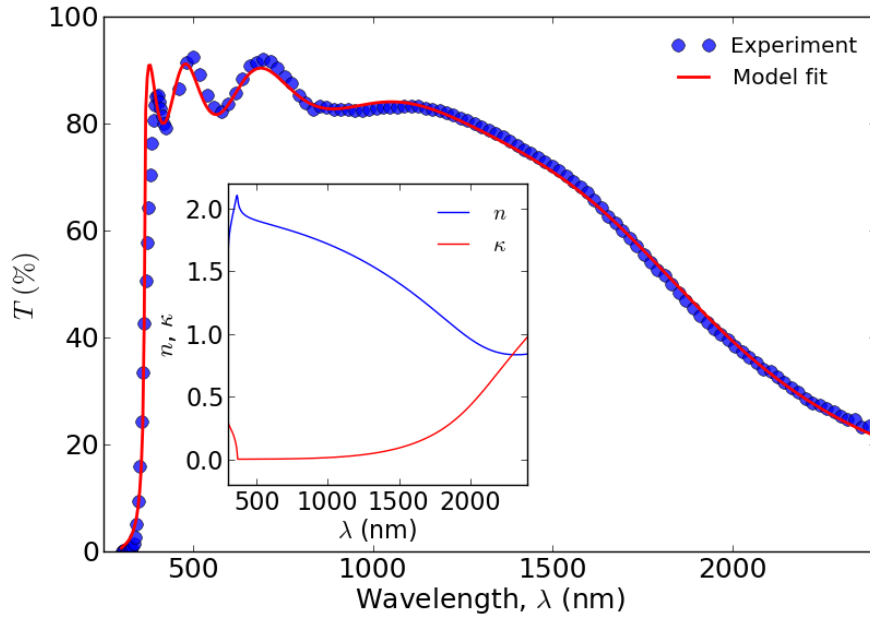


FIG. 1.

FIG. 2.

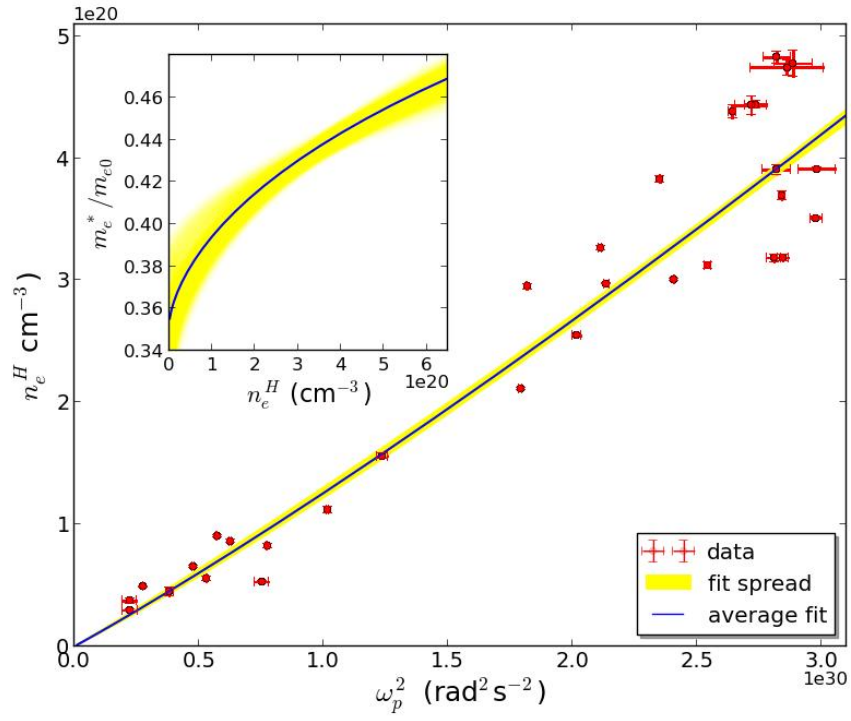


FIG. 3.

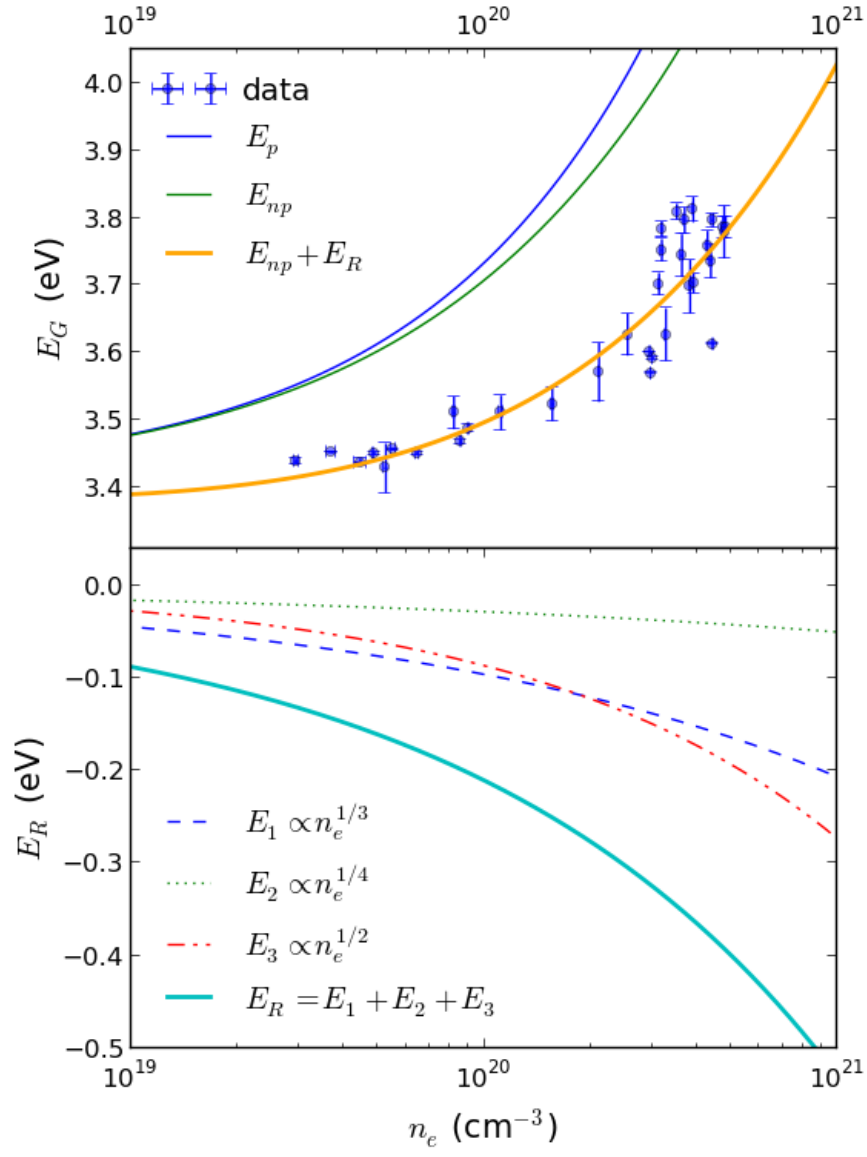


FIG. 4.

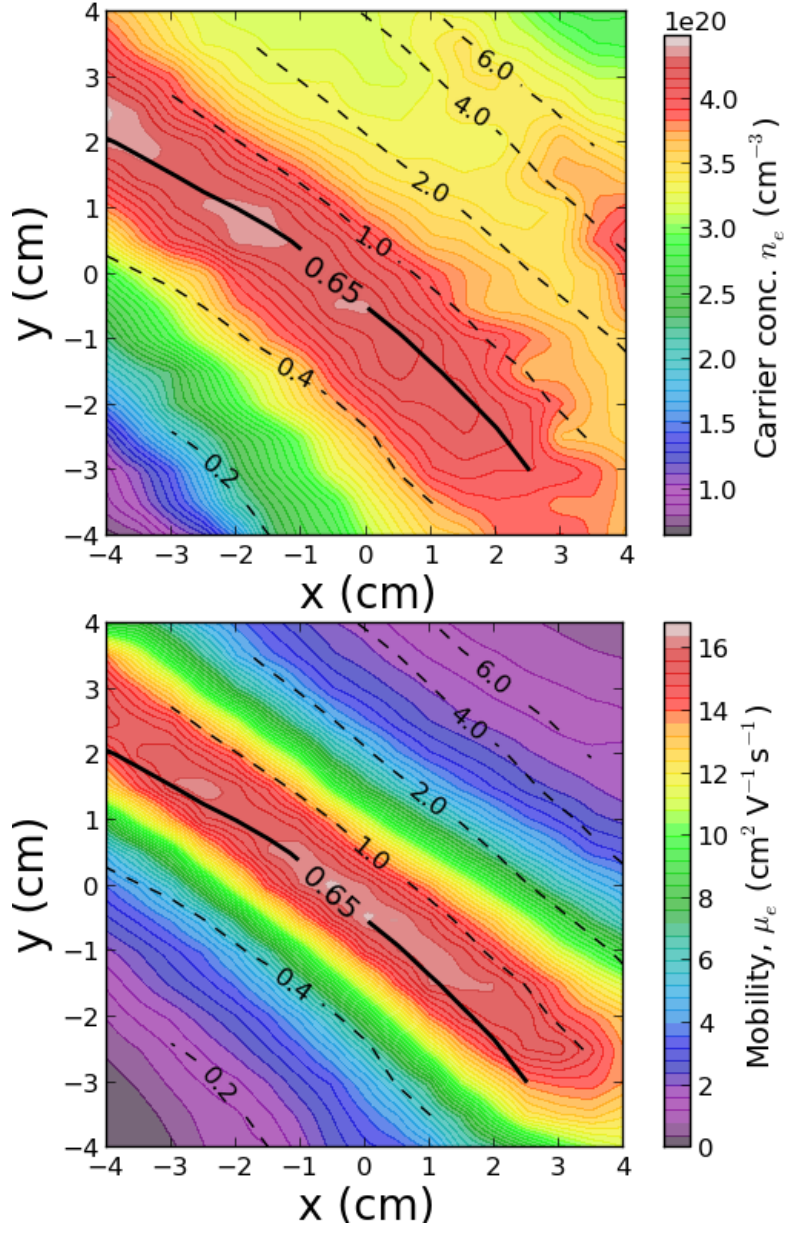


FIG. 5. Contour maps of carrier concentration and mobility over the combinatorial sample. The (–) contour lines show an overlay of the % wt. SiO₂ composition.

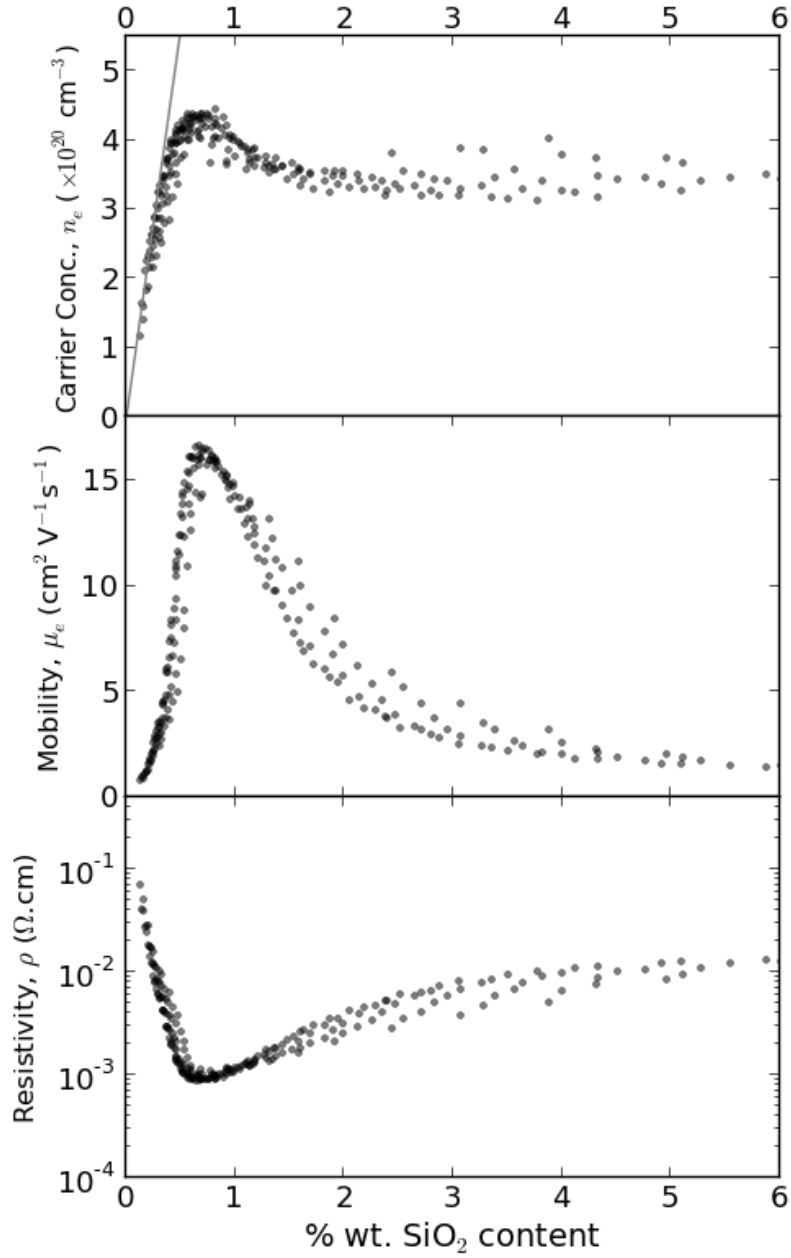


FIG. 6. Distributions of carrier concentration, mobility and resistivity with respect to % wt. SiO₂ content. The maximum values for n_e ($4.4 \times 10^{20} \text{ cm}^{-3}$) and μ_e ($16.5 \text{ cm}^2 \text{ V}^{-1} \text{ s}^{-1}$) coincide with a composition of 0.65% wt. SiO₂. The solid straight line in the top plot shows the maximum theoretical carrier concentration with respect to SiO₂ content should every incorporated Si atom be substituted at a Zinc site and donate 2 carriers.

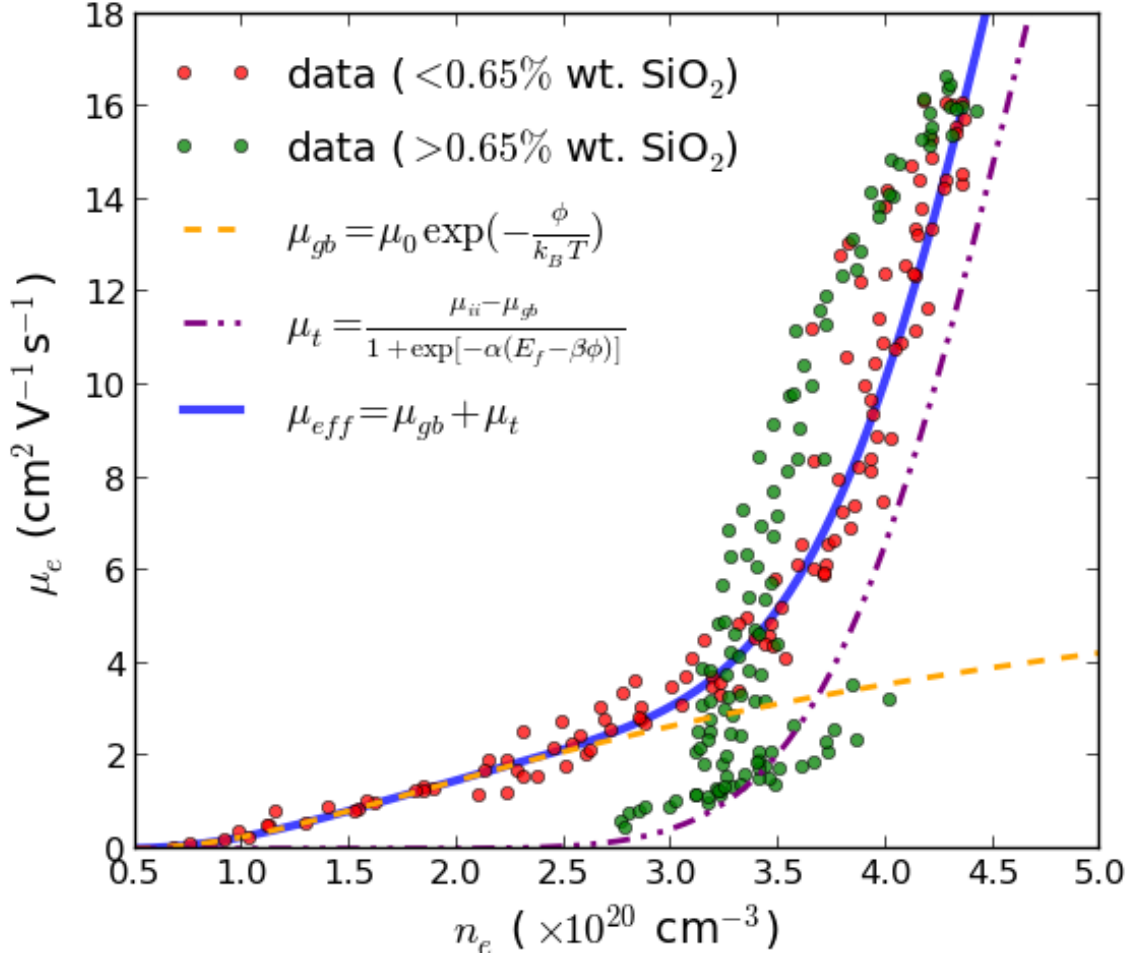


FIG. 7.

Parameter 1	Extracted Value	Copmparison [14]
$A (\times 10^{-8} \text{ eV.cm})$	2.1 ± 0.8	0.69
$B (\times 10^{-7} \text{ eV.cm}^{3/2})$	3.0 ± 2.6	1.6
$C (\times 10^{-7} \text{ eV.cm}^{3/4})$	8.7 ± 1.5	7.76
$E_{G0} (\text{eV})$	3.41 ± 0.01	-

TABLE I. This is the caption